Ground settlements above tunnels in fractured crystalline rock: numerical analysis of coupled hydromechanical mechanisms

C. Zangerl · E. Eberhardt · S. Loew

Abstract Vertical settlements with magnitudes reaching 12 cm were measured in fractured crystalline rock several hundred metres above the Gotthard highway tunnel in central Switzerland. Such magnitudes of surface subsidence were unexpected, especially in granitic gneisses and appear to be related to large-scale consolidation of fractures resulting from fluid drainage and pore pressure changes following tunnel construction. This paper focuses on the mechanisms involved in the development of such surface displacements and presents the preliminary results of 2-D discontinuum (i.e. distinct-element) and 2-D continuum modelling (i.e. finite-element). Results show that settlements are most sensitive to horizontal joints, as would be expected, but that vertical fractures also contribute to the settlement profile through a 'Poisson ratio' effect. However, these models also suggest that fracture deformation alone cannot explain the total subsidence measured. As such, 2-D poro-elastic finite-element models are presented to demonstrate the contributing effect of consolidation of the intact rock matrix.

Résumé Des tassements verticaux atteignant 12 cm ont été mesurés dans des roches cristallines fracturées à plusieurs centaines de mètres au-dessus du tunnel routier du Gothard en Suisse centrale. De tels ordres de grandeur de subsidence de la surface sont inattendus, en particulier dans des gneiss granitiques et paraissent liés à une consolidation à grande échelle des fractures résultant du drainage du fluide et des variations de la pression porale après le creusement du tunnel. Cet article s'intéresse aux mécanismes impliqués dans le développement de tels déplacements de la surface et présente les résultats préliminaires d'une modélisation d'un discontinuum en 2-D ("distinct-element") et d'un continuum en 2-D ("finite-element"). Les résultats montrent que les tassements sont plus sensibles sur les discontinuités horizontales, comme c'était prévu, mais que les fractures verticales contribuent également au profil de tassement selon un effet de 'taux de Poisson'. Toutefois, ces modèles laissent également penser que la déformation des fractures seule ne peut pas expliquer la totalité de la subsidence mesurée. Aussi des modèles de poro-élasticité en 2-D aux éléments finis sont présentés pour démontrer l'effet contributif de consolidation de la matrice de la roche intacte.

Resumen Se han registrado asentamientos verticales de hasta 12 cm en rocas cristalinas fracturadas situadas centenares de metros por encima del túnel de la autopista del Gotardo, en el centro de Suiza. Tales magnitudes de subsidencia superficial son inesperadas, sobretodo en un gneis granítico, y parecen estar relacionadas con la consolidación a gran escala de las fracturas resultantes del drenaje de fluidos y de los cambios de presión intersticial resultantes de la construcción del túnel. Este artículo se centra en los mecanismos involucrados en el desarrollo de los desplazamientos superficiales, y presenta los resultados preliminares de modelos bidimensionales discontinuos ("distinct-element") y continuos ("finite-element"). Se muestra que los asentamientos son más sensibles a las diaclasas horizontales, como es de esperar, pero también que las fracturas verticales contribuyen al perfil de asentamientos mediante un efecto de 'relación de Poisson'. Sin embargo, estos modelos sugieren también que la deformación de fracturas no puede explicar por sí sola la subsidencia total medida. Se presenta los modelos poroelásticos en diferencias finitas que demuestran la contribución a la consolidación por parte de la roca matriz intacta.

Keywords Crystalline rock · Fractured rocks · Hydromechanically coupled · Subsidence

Received: 27 April 2002 / Accepted: 28 October 2002
Published online: 15 January 2003

© Springer-Verlag 2003

C. Zangerl (✉) · E. Eberhardt · S. Loew
Engineering Geology,
Swiss Federal Institute of Technology (ETH Zurich),
Hoenggerberg 8093, Zurich, Switzerland
e-mail: zangerl@erdw.ethz.ch
Tel.: +41-1-6332717, Fax: +41-1-6331108

Introduction

Settlements in fractured crystalline rocks are rarely observed and in the past engineers would not expect substantial subsidence to be generated above a deep-seated tunnel. Large-scale displacements in such projects can have a negative influence on surface structures especially with respect to concrete dams, bridge piers and abut-

 DOI 10.1007/s10040-002-0234-4

Fig. 1 Location map with study area

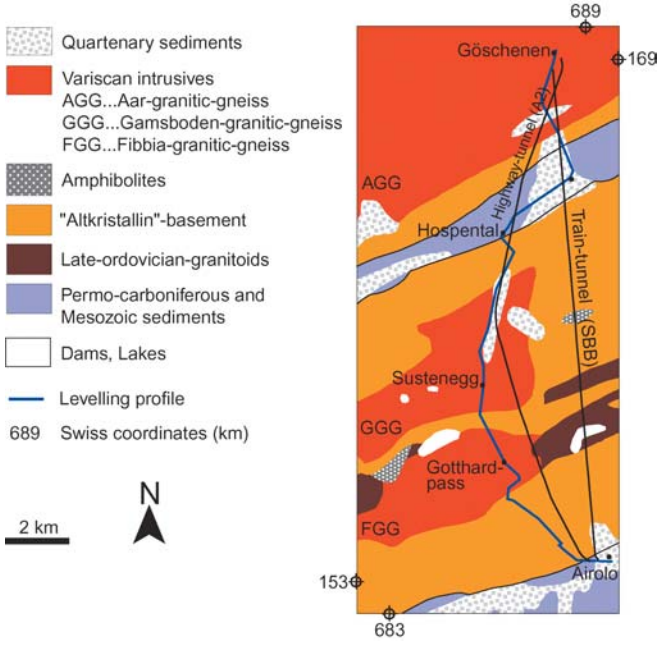

Fig. 2 Geological map of Gotthard region

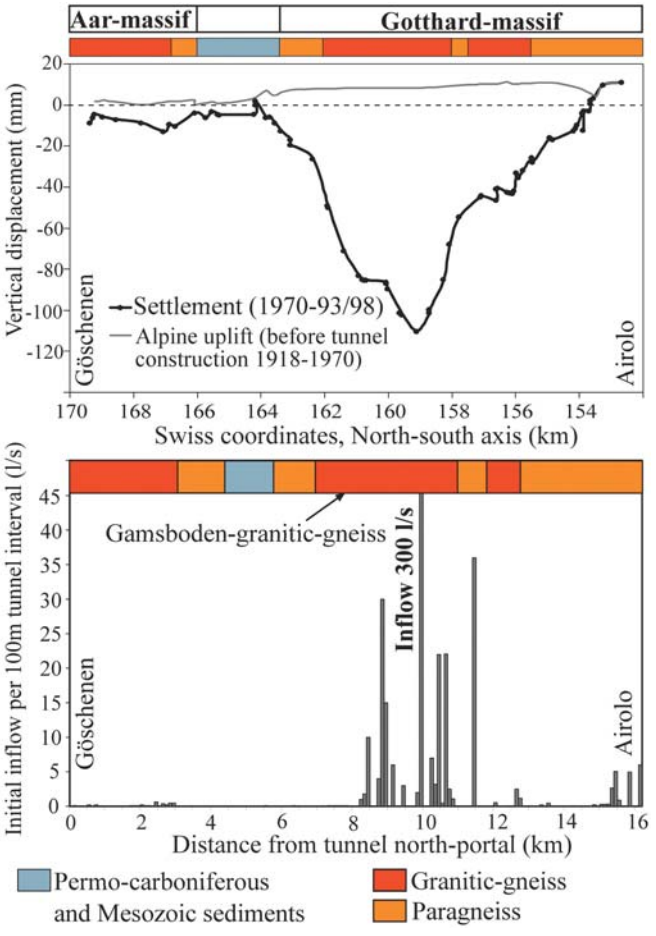

Fig. 3 Surface subsidence in the time interval 1970 to 1993/1998 and Alpine uplift (*upper diagram*). Early time water inflow rates into A2 road tunnel (*lower diagram*)

ments, and other subsidence sensitive structures. For example, subsidence-induced cracks if generated may threaten the integrity of these structures leading to costly repairs and/or possible failure (e.g. see the Zeuzier Dam, Lombardi 1988).

Recent high-precision levelling measurements of surface displacements along the Gotthard pass road in central Switzerland have revealed up to 12 cm of subsidence along sections that pass several hundred metres above the Gotthard A2 highway tunnel (Fig. 1 and 2). The Swiss Federal Office of Topography carried out the levelling measurements in 1993/1998 as a closed loop over the old Gotthard-pass road and through the A2 road tunnel. Two earlier measurement campaigns were made along this N–S profile over the old Gotthard pass road in 1918 and 1970. During the time interval between 1918 and 1970 (i.e. before tunnel construction), an undisturbed alpine uplift with a rate of 1 mm/year was detectable (Fig. 3). This uplift rate concurs with estimated rates of 0.6 mm/year as determined using fission-rack techniques (Kohl et al. 2000). In contrast, the time interval between 1970 and 1993/1998 (i.e. after tunnel construction) shows significant downward displacements along a 10-km region above the tunnel (Fig. 3).

The close spatial proximity between maximum tunnel inflow rate and maximum settlement (Fig. 3) and the temporal relationship between tunnel construction and settlement clearly shows causality between water drainage into the tunnel and surface deformation. Localised surface processes, e.g. creeping landslides or flexural toppling, could be excluded as alternative explanations given the absence of local indicators and the extent over which the settlements were measured (10 km along a N–S line, roughly parallel to the tunnel axis; see Fig. 2).

Maximum settlements and high initial inflow rates into the tunnel (Fig. 3) were measured along sections involving heavily fractured granitic–gneiss (Gamsboden granitic–gneiss). Of surprise was the relatively small tunnel interval over which the high initial inflow rates occurred (3 km) relative to the measured settlement trough (10 km). Subsidence of this magnitude in a frac-

 DOI 10.1007/s10040-002-0234-4

tured crystalline rock mass would not generally be expected and appears to be related to large-scale consolidation resulting from fluid drainage and pore-pressure changes in the rock mass (i.e. fractures and intact rock).

A more detailed description of the problem can be found in Zangerl et al. (2001). The hydrogeological situation in the Gotthard area is described in Loew (2001) and Lutzenkirchen (2002). This paper presents the first results of a comprehensive modelling exercise and focuses on the mechanisms involved in the development of such surface displacements through the application of a 2-D-coupled hydromechanical discontinuum modelling using the distinct-element code UDEC (Itasca 1999). In addition, 2-D poro-elastic continuum modelling of the intact rock material and smaller-scale fractures is included using the finite-element program VISAGE (VIPS 2001). All models presented in this paper are generic and conceptual. Realistic site-specific models, which honour the local topographical, geological and hydrological conditions, and are calibrated with the site-specific hydromechanical observations, are to be presented in subsequent papers.

Flow and Deformation Models for the Underlying Subsidence Mechanisms

Fluid Flow and Fluid Pressure

The excavation of a tunnel in a water-saturated fractured crystalline rock mass enables inter-connected brittle fault zones and joints to drain. Initially this quick fluid drainage would cause a drop in water pressure along fractures adjacent to the tunnel. In a later stage, the pressure change would penetrate more deeply into the rock mass, lowering the phreatic water table until a new equilibrium between water inflow into the tunnel and far-field water recharge is reached. In addition to the drainage of the more permeable fracture network, pore pressures in the low-permeability intact rock matrix will slowly adjust to the new boundary conditions. The time taken to reach equilibrium between the fluid pressure in the fractures and the fluid pressure in the intact rock matrix is strongly dependent on the matrix block size and the hydraulic diffusivity.

These pore pressure changes will affect the effective stress conditions, which, in turn, influence the hydraulic flow field either through variations in the fracture aperture or the porosity within the intact rock matrix. A decrease in the mechanical aperture (i.e. fracture width) as a result of pore pressure change also means a decrease in the hydraulic aperture and, thus, a decrease in the permeability of the fractures. This aperture–flow coupling relationship is often represented by the cubic law equation for laminar flow between two parallel plates with smooth surfaces:

$$Q = \frac{ga^3}{12v}\frac{dp}{dl}w \tag{1}$$

where Q =flow rate, g = gravitational acceleration constant, a = mean fracture aperture, v = kinematic viscosity of the fluid, dp/dl = hydraulic gradient and w = fracture width in the direction of flow.

Given the simplifying assumptions in its formulation, it must be questioned whether the cubic law is valid for fluid flow in fractures with large aperture and hydraulic gradient around the tunnel. In addition, Pyrak-Nolte and Morris (2000) suggest that stress alone is not the link between hydraulic and mechanical fracture properties. Instead, they suggest that the fracture geometry and how it deforms under stress provides this link. Regardless, the cubic law provides a simple and numerically efficient approximation to laminar fluid flow in fractures. As such, the cubic law was used in this study, in part, to model deformation mechanisms relating to pore pressure changes. Furthermore, as the quantification of inflow rates into the tunnel was not an objective of this study, limitations relating to the use of the cubic law relationship are reduced. In UDEC, the fractures are viewed as defining a network of interconnected voids and channels that will be referred to as 'domains' (Itasca 1999). Changes of domain pore pressures were calculated, taking into account the net flow into the domain, and possible changes in domain volume due to the incremental motion of the surrounding blocks. The pore pressure change Δp is represented by:

$$\Delta p = \frac{K_w}{V}\left(\sum Q \cdot \Delta t - \Delta V\right) \tag{2}$$

where ΣQ is the flow into the node, ΔV is the mechanical volume change, K_w is the bulk modulus of the fluid and Δt is the time step. Fracture deformation and hydraulic apertures were calculated as a function of the effective stresses and normal stiffness of the joints. The hydraulic aperture, a, is given by:

$$a = a_0 + u_n \tag{3}$$

where a_0 is the aperture at zero normal effective stress and u_n is the contact normal displacement (convention: fracture closure represented by negative number). A minimum value, a_{res}, is assumed for an aperture beyond which mechanical closure does not affect the contact permeability.

Deformation Models

Three different fracture-based hydromechanical deformation models were developed for this study. These models and their respective roles in generating the settlements measured above the Gotthard tunnel were analysed using discontinuum modelling techniques (i.e. the distinct-element method). A fourth deformation model based on microfracture permeability and poro-elastic consolidation of the intact rock matrix was also developed and analysed using continuum finite-element techniques (note that the distinct-element formulation employed by the code UDEC does not allow for fluid flow within the intact blocks, treating them as impermeable).

Each of the deformation models involves either drainage of water-filled discontinuities and/or drainage of the intact rock. Water-filled discontinuities change their me-

 DOI 10.1007/s10040-002-0234-4

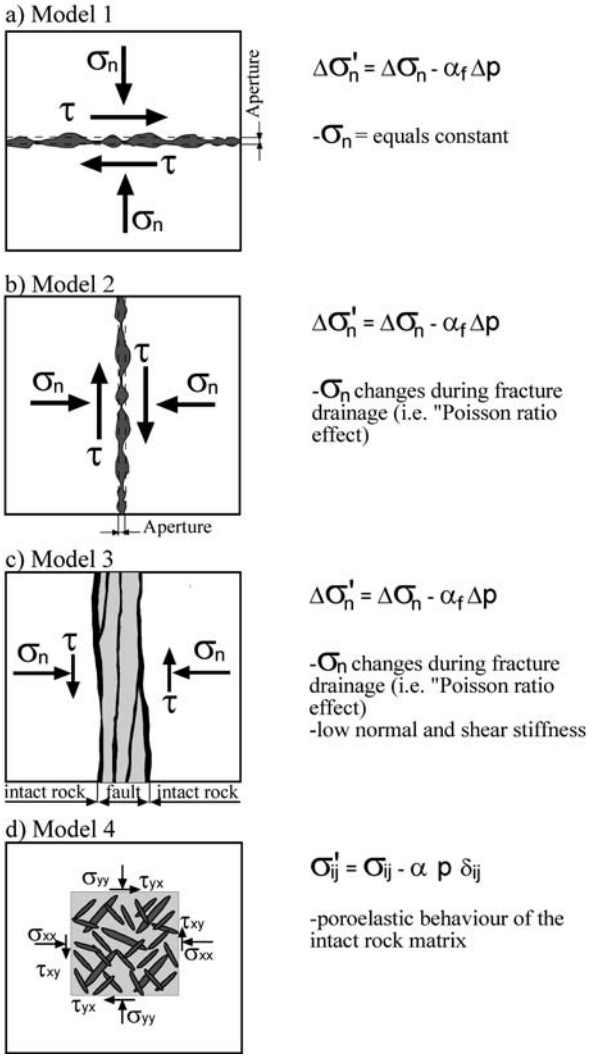

Fig. 4 Conceptual models showing mechanical response to fluid drainage of **a** horizontal joints, **b** vertical joints, **c** vertical faults and **d** intact rock

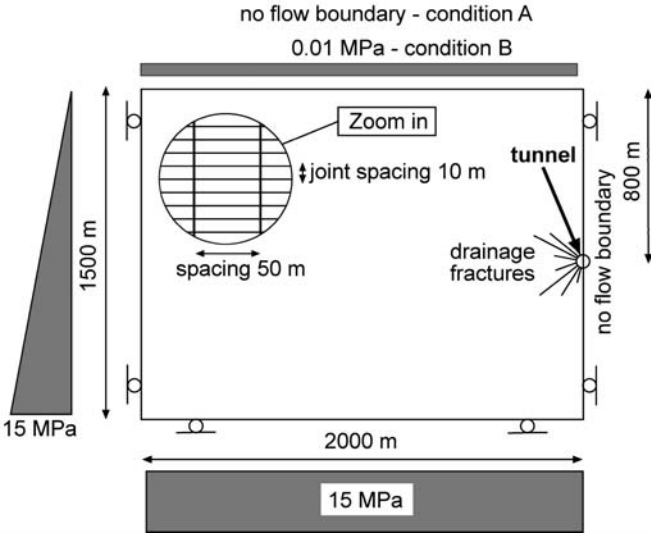

Fig. 5 Distinct-element model geometry and boundary conditions

chanical aperture during pore-pressure drops as can be shown through the effective stress law for fracture closure:

$$\Delta\sigma_n' = \Delta\sigma_n - \alpha_f \cdot \Delta p_w \quad (4)$$

where σ'_n = effective normal stress, σ_n = total normal stress, α_f = effective stress coefficient and Δp_w pore pressure (Robin 1973).

The four deformation models can be described as follows:

1. Horizontal joint-controlled: intuitively horizontal joint closure through water-pressure decrease would contribute the most towards vertical settlements. In this deformation model the total normal vertical stress is assumed to stay constant (or varies only a little during this process); only a change in the normal effective stress across the fracture takes place (Fig. 4a). As such, the deformation model does not rely on deformation of the intact rock blocks.
2. Vertical joint-controlled: in contrast, vertical joint closure during the drainage process will affect both the total and effective normal stress acting horizontal to the fracture plane. This change in the horizontal total normal stress with the vertical stress remaining constant would subsequently generate strains within the intact rock blocks (Fig. 4b). As such, they should experience shortening in the vertical direction and expansion in the horizontal direction (i.e. Poisson's ratio effect).
3. Vertical brittle fault zone-controlled: deformation model 3 is similar to model 2, but substitutes the hydromechanical properties of the vertically aligned joints for those of vertical brittle fault zones (based on field mapping observations; Zangerl et al. 2001). This differentiation is important given that shear and normal stiffness values for the brittle fault zones are much lower than those for unfilled joints (Fig. 4c).
4. Intact rock matrix-controlled: deformation model 4 explains the surface deformation by applying the theory of linear poro-elasticity to intact low-permeability rock blocks. The effective stress law for a homogeneous poro-elastic continuum can be described as:

$$\sigma_{ij}' = \sigma_{ij} - \alpha p \delta_{ij} \quad (5)$$

where σ'_{ij} = effective stress; σ_{ij} = total stress, α = Biot's constant, p = pore pressure and δ_{ij} = Kroenecker's delta (Nur and Byerlee 1971). In this case, pore space and permeability are attributed to microfractures in the crystalline rock matrix (Fig. 4d). Values reported for Westerly and Charcoal granite by Detournay and Cheng (1993), together with recent laboratory tests performed on granitic gneiss from the Gotthard study area, would seem to indicate that some poro-elastic

 DOI 10.1007/s10040-002-0234-4

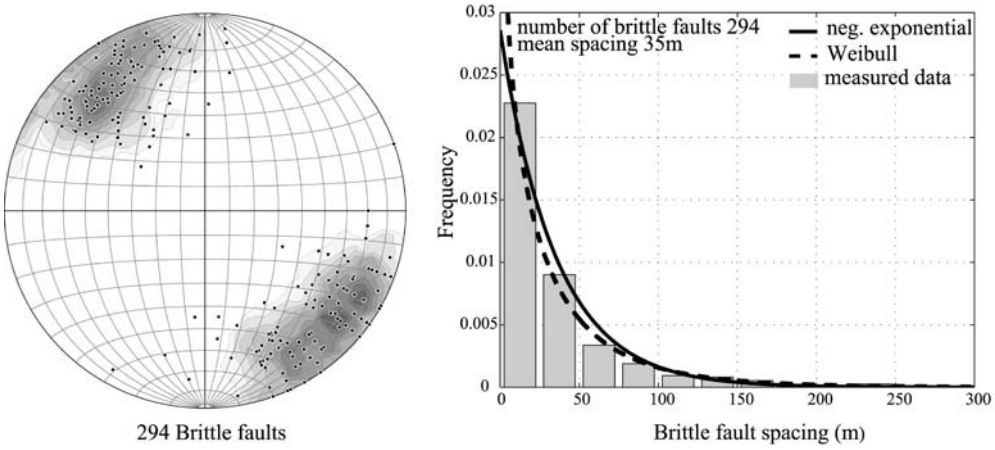

Fig. 6 Contoured pole plots showing brittle fault zone orientations (*left*) and corresponding total spacing histograms (*right*)

deformation could be expected during pore pressure changes within the intact rock matrix. However, these studies are currently ongoing and are not discussed in detail in this paper.

Discontinuum Modelling

Model Geometry

Based on the first three deformation models outlined above, two sets of continuous, orthogonal (i.e. horizontal and vertical), fully persistent discontinuities were used to form the fracture network. The model is two-dimensional and assumes half-symmetry with a width of 2,000 m and a height of 1,500 m (Fig. 5). This model geometry was selected after studying the influence of boundary effects using a model with an extended width of 4,000 m. A 20-m diameter tunnel was placed at 800 m depth, with eight radial joints added to promote deeper hydraulic interaction. Joint spacing in the orthogonal fracture pattern relates to surface scan-line data from the Gamsboden granitic–gneiss (Zangerl et al. 2001). The mean joint normal-set spacing measured on surface ranges from 0.5–1.5 m for both horizontal and vertical joints. Joint data sets from the Gotthard tunnel show that joint spacing increases with depth. Brittle fault zones mapped from the tunnel show a strong preferred orientation (strike direction perpendicular to tunnel axis) and a mean spacing of 35 m (Fig. 6).

The direct application of field discontinuity data, however, can result in extremely complex models that are unmanageable in terms of computer memory requirements and solution run times. A balance, therefore, must be found between reproducing the important geological elements (and their effect on the modelled mechanisms), and developing a model that is numerically efficient. As such, the mean joint spacing used in the UDEC models was set to 10 m for horizontal joints and 50 m for vertical joints and faults. By adopting a horizontal joint spacing where ten joints mapped in the field are replaced by one joint, the properties of the one modelled joint are scaled to those representative of the bulk rock mass (Fig. 7 as described in the next section).

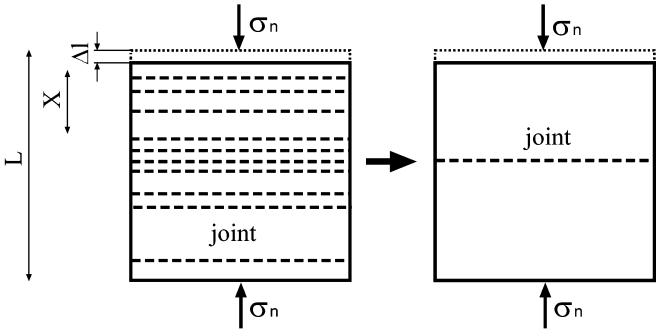

Fig. 7 Scaling of multiple joint properties to those representative of the bulk rock mass

Table 1 Intact rock properties for discontinuum models

Material	Parameter	Value
Intact granite	Young's modulus, E	50 GPa
	Poisson's ratio, ν	0.25
	Density, ρ	2,700 kg/m^3

Material Properties

All models were solved assuming an elastic constitutive model for the intact block material. Plastic strains would only be expected, at most, along the tunnel periphery <0.5 m into the rock mass and, given the 800-m overburden height between the tunnel boundary and surface, were assumed to be insignificant. The selection of an elastic constitutive material model effectively restricts the subsidence-generating deformation mechanisms to those produced through elastic strain of the intact blocks and shear and normal displacements along fractures. Material properties for the intact block parameters were selected based on typical values for granite (Table 1).

Intuitively, it is expected that the normal stiffness of joints and/or brittle fault zones would have the largest influence on the calculated subsidence. A detailed literature study, therefore, was performed to review joint normal deformation behaviour in granitic rocks. Most published studies report laboratory-derived normal stiffness

 DOI 10.1007/s10040-002-0234-4

Table 2 Joint and brittle fault zone properties

Property	Joint	Brittle fault zone
Normal stiffness	Stress-dependent (see Fig. 7)	Stress-independent (varied from 0.1 to 100 GPa/m)
Shear stiffness	10 GPa/m	1 GPa/m
Cohesion	0 MPa	0 MPa
Friction angle	30°	20°
Zero stress aperture	0.6 mm (represents 10 joints)	1.5 mm (represents one fault zone)
Residual aperture	0.3 mm (represents 10 joints)	0.5 mm (represents one fault zone)
Rock mass equivalent Hydraulic conductivity	2×10^{-6} m/s (parallel to joints)	2×10^{-6} m/s (parallel to faults)

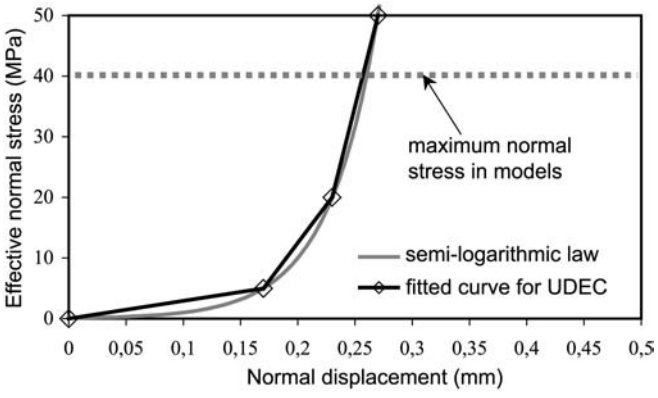

Fig. 8 Normal deformation law for one single joint

values for natural or artificially generated granitic joints (e.g. Sun et al. 1985; Makurat et al. 1990; Bart et al. 2000). Only a few tests report values that are measured in situ (e.g. Pratt et al. 1977; Makurat et al. 1990). These tests show a strong non-linearity in the normal stress–normal displacement relationship, with a wide range of maximum joint closure values.

The semi-logarithmic law, proposed by Bandis et al. (1983) for unmated joints, was chosen in this study to represent the behaviour of modelled joint closure.

$$\log(\sigma_n') = q \cdot \Delta v + p \tag{6}$$

where σ'_n = joint effective normal stress; q and p = constants (for this study q=10; p=-1) and Δv = joint normal deformation (i.e. closure). This law was fitted to several tests from the literature and their parameters established. Implementation into UDEC required that the semi-logarithmic law be represented as four points along the normal stiffness curve. Figure 8 shows the joint displacement curve derived from laboratory and in-situ measurements for a single joint and additionally the four points implemented into UDEC to represent the curve.

Published studies pertaining to normal deformation behaviour of brittle fault zones are more limited than those for joints. Only a few data sets were found in the literature. Martin et al. (1990) report values for a brittle fault zone consisting of fractures, fault breccias and clay-gouge in the Lac du Bonnet granite batholith at the URL-test site in Canada. The test was conducted in a 96-mm-diameter borehole with a specially developed packer system (PAC-ex-system). Results from this test report a stress independent normal stiffness with relatively low values between 2–6 MPa/mm. Given the small stress interval applied in these tests (0–2 MPa), such values must be used with caution. Similar values, however, were also reported by Infanti and Kanji (1978) for clay-filled joints with normal stiffness values ranging between 0.1–5 MPa/mm depending on the thickness of the clay filling. They too concluded a stress-independent normal stiffness. In contrast, higher values (approximately an order of magnitude stiffer) were measured in situ by Majer et al. (1990) at the Grimsel Rock Laboratory in central Switzerland, for two granite-hosted ductile shear zones overprinted by minor brittle deformation.

An additional consideration with respect to joint normal stiffness is its relationship with mean fracture spacing as deformation-controlling parameters. As such, the extent of deformation may be controlled either by varying the mean spacing or normal stiffness. This proves valuable for simplifying large models where realistic field measured spacing values would lead to an unmanageable number of blocks. However, it is important to keep in mind that this relationship is only valid for constant normal stress. An example of its use in the UDEC models is demonstrated in the selection of a 10-m spacing for the horizontal joints in contrast to the 1-m mean spacing measured in the field. Thus one modelled joint represents ten joints in terms of their bulk normal stiffness and deformation characteristics (Fig. 7). The following equation shows this relationship:

$$\Delta l = \frac{L}{X} * \frac{\sigma_n}{k_n} \quad \text{which yields:} \quad k_{n1} * X_1 = k_{n2} * X_2 \tag{7}$$

where Δl = normal deformation; L = block length; X = mean spacing; σ_n = constant normal stress and k_n = normal stiffness. Normal stiffness values derived through this procedure are given in Table 2. Shear stiffness values were assumed to be constant (i.e. non-stress dependent) with values for joints and brittle fault zones based on those given by Bandis et al. (1983). A rock mass hydraulic conductivity of 2×10^{-6} m/s is calculated from residual fracture apertures in vertical and horizontal direction and the cubic law (Eq. 1). Such values are indicative for medium permeable fault zones in the Gotthard area. Conductivity values observed in an intact fractured granitic rock mass are typically two magnitudes lower (Loew 2001).

 DOI 10.1007/s10040-002-0234-4

Boundary and Initial Conditions

Initial total stress conditions were set to K=1 (horizontal to vertical stress ratio equals one), with vertical stresses determined by gravitational loading. Initial hydrostatic pore pressures were set by assuming a groundwater table at the surface (Fig. 5). The effective stresses in the fractures were initialised as the difference between the normal component of the initial total stress acting across the discontinuity plane and the initial pore pressures within the discontinuity.

Two different models in terms of hydraulic boundary conditions were established. All models were solved assuming steady-state conditions and the pore pressures were calculated as relative pressures (i.e. 0 Pa in UDEC models were equivalent to atmospheric pressure). The first condition represents a free water surface with no recharge, which allows drawdown due to tunnel drainage (boundary condition A). Depending on the frequency and hydraulic apertures of the fractures (i.e. the equivalent rock mass hydraulic conductivity), the phreatic surface could drop down as far as the tunnel elevation. This condition, therefore, represents the maximum pore-pressure drop that could be achieved in the rock mass. Whether probable or not, this condition was chosen so that each discontinuum model could be directly compared with one another (e.g. deformation model 1 vs 2, 2 vs 3, etc.). By modelling a similar redistribution of pore pressures in each case, a more direct comparison could be made between the resulting subsidence profiles.

The second hydraulic boundary condition involves a fixed water level that allows drainage of the rock mass around the tunnel, but without changing the water table (boundary condition B). The reason for establishing this condition was to check if for a more limiting drainage condition, i.e. one that would not alter surface groundwater conditions (e.g. springs), considerable surface subsidence could still result. Based on field observations, it is believed that condition A is the more likely situation for highly permeable structures (i.e. a network of brittle fault zones or fracture zones) that, locally, allow large values of drawdown. In contrast, boundary condition B can be applied to models where, on a regional scale, negligible changes in the water surface occur mainly due to direct infiltration from surface water bodies and a strong recharge. Both types of boundary conditions are discussed in more detail in Loew (2002).

Continuum Modelling

Model Development

For the fourth deformation model, that of poro-elastic consolidation of the intact rock matrix (Fig. 4d), a 2-D finite-element model was generated. The same model geometry/dimensions were used as those for the discontinuum models, but calculated as a full model (Fig. 9). Similarly, the intact rock properties, in situ stresses and boundary conditions were kept the same. Values for the Biot's and Skempton coefficients, α and β, were chosen to allow maximum consolidation for the prescribed permeability. The water-table level along the top of the model was fixed in the same manner as 'boundary condition B' described for the discontinuum models. This meant that drainage would be restricted to the rock mass immediately surrounding the tunnel, and no drawdown of the water surface occurs. The permeability values used in the continuum models were based on those for an intact fractured granitic rock mass (i.e. without fault zones). Given that the aim of the continuum modelling was to study the poro-elasticity effects of the intact rock matrix, mechanical and hydraulic input parameters (i.e. Young's modulus, Poisson's ratio and hydraulic conductivity) were defined according to intact granitic rock. These values are summarised in Table 3.

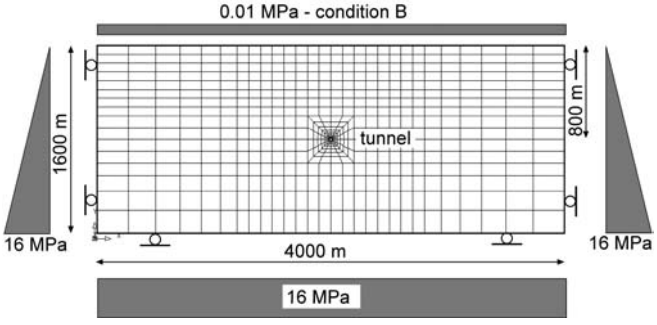

Fig. 9 Finite-element model geometry and boundary conditions

Table 3 Intact rock properties for continuum models

Material	Parameter	Value
intact granite	Young's modulus, E	50 GPa
	Poisson's ratio, ν	0.25
	density, ρ	2,700 kg/m^3
	Biot's coefficient, α	1.0
	Skempton's coefficient, β	1.0
	Hydraulic conductivity, K_{xx}=K_{yy}	10^{-8} m/s

Results and Discussion

Boundary Condition A: Groundwater Drawdown to Tunnel Level

Each UDEC model presented in this paper includes both vertical and horizontal fractures. Depending on the deformation models tested, the normal stiffness of the vertical and horizontal fractures was varied and its effect on surface displacements calculated. For the first model series (boundary condition A), a free water surface was assumed enabling drawdown of the water table close to the tunnel level. After setting the initial stress and fluid pressure conditions and cycling them to equilibrium, the tunnel was opened allowing fluid flow (i.e. drainage). The resulting pore-pressure drop throughout the fracture network (Fig. 10), in turn, generated vertical and horizontal block displacements.

Horizontal joints, as was expected, were found to have the biggest influence on subsidence. Depending on the

 DOI 10.1007/s10040-002-0234-4

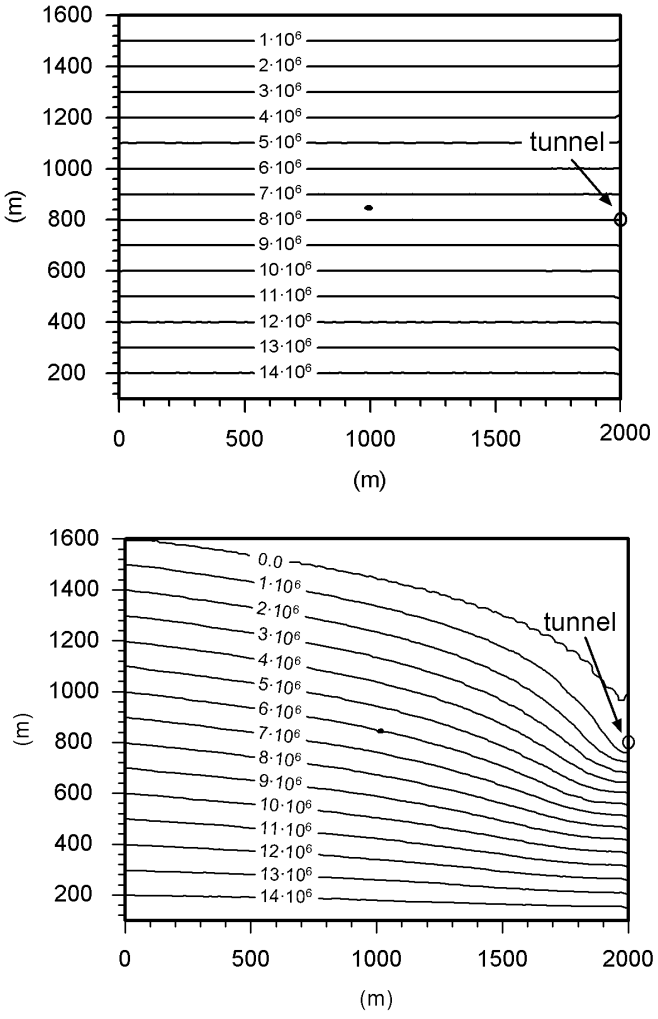

Fig. 10 Pore-pressure distribution (units in Pa) before (*upper*) and after (*lower*) tunnel drainage for groundwater drawdown close to tunnel level (boundary condition A). The 0.0-Pa pressure line represents the boundary between the saturated and unsaturated zone in the model. The maximum pore pressure calculated directly above the tunnel reaches only 2×10^{-5} Pa

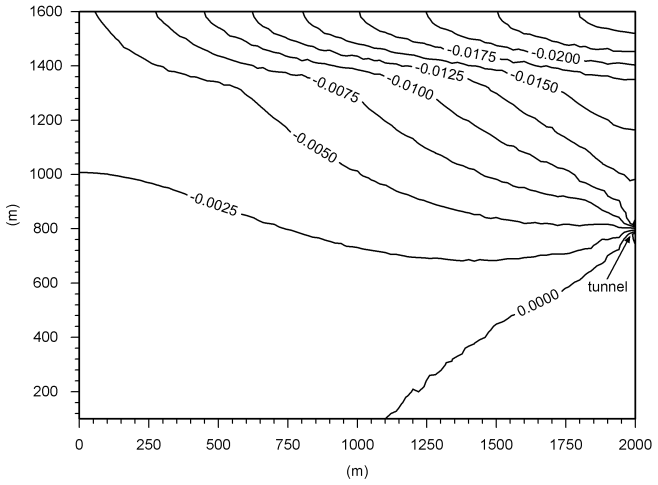

Fig. 11 Vertical subsidence (in metres) for horizontal joint-controlled model (conceptual model 1)

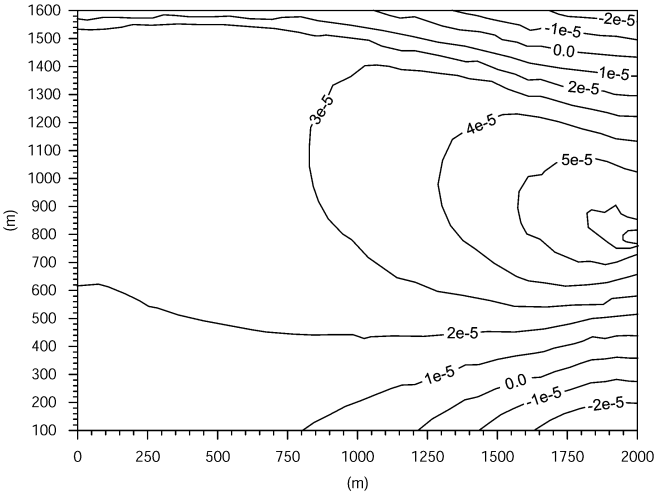

Fig. 12 Horizontal strains for vertical brittle fault zone-controlled model (conceptual model 3)

values of normal stiffness or mean joint spacing used, surface settlements ranging between 0.005–0.22 m were modelled. For example, implementing an exceptionally low normal stiffness (k_n=0.3 MPa/mm between 0 and 5 MPa normal stress) resulted in a maximum settlement of 0.22 m. If a more realistic normal stiffness curve was used, and scaled to represent the stiffness of ten joints within a 10-m interval (k_n=3 MPa/mm between 0 and 5 MPa normal stress), the settlements only reach 0.03 m (Fig. 11). The shape of the settlement trough in the model plane (i.e. perpendicular to the levelling profile) was generally flat, extending towards the left model boundary (i.e. away from the tunnel), with vertical displacements still reaching up to 20% of the maximum value 1,500 m from its centre. The point of maximum settlement in these models was observed directly above the tunnel.

Similar results were obtained for models focusing on vertical joint and vertical brittle fault zone mechanisms contributing to surface settlements (i.e. deformation models 2 and 3). Maximum settlements of only 0.036 m were calculated. The corresponding decrease in total horizontal and vertical stress throughout the model was found to be less than 2 MPa. Only in the immediate area surrounding the tunnel was a larger stress change observed. As hypothesised and described in reference to the deformation models, the modelled strains depict closure of the vertical fractures and horizontal expansion of the intact blocks, i.e. the Poisson ratio effect (Fig. 12).

In comparison, modelled intact block strains in the vertical direction clearly show expansion below and partly above the tunnel and contraction throughout the rest of the model (Fig. 13). The maximum amount of vertical shrinkage is located several hundred metres away from the tunnel. Positive and small negative vertical intact block strains above and below the tunnel (i.e. showing mainly expansion) are mostly due to the tunnel

 DOI 10.1007/s10040-002-0234-4

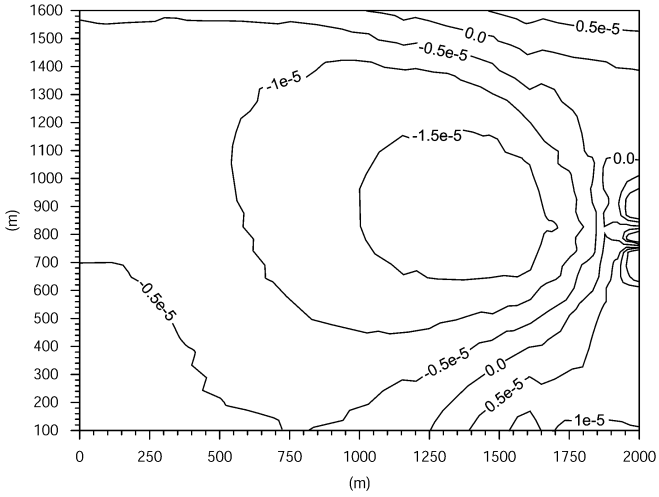

Fig. 13 Vertical strains for vertical brittle fault zone-controlled model (conceptual model 3)

excavation and the pore-pressure decrease near the tunnel. Horizontal joint closure due to changes in the vertical effective stress continuously increases from the left to the right model boundary and generates vertical shear deformation between adjacent columns of blocks. Directly above and below the tunnel, the amount of shear displacement along vertical fractures is small in comparison to horizontal joint closure. Fractures located further away from the tunnel show the opposite behaviour. They are characterised by large shear deformation combined with small, horizontal joint closure (Fig. 14). Low values of vertical shear deformation, together with large values of horizontal joint closure, results in vertical expansion of the intact blocks. In contrast, large shear displacements, combined with minor closure of the horizontal joints, creates vertical block shrinkage and horizontal expansion. The amount of shear offset shown in Fig. 14 results from the summation of horizontal joint closure values along a column of blocks and does not originate from deformation on one single fracture. Within the model, shear occurs at elastic deformation conditions (i.e. no shear failure occurred), attaining maximum val-

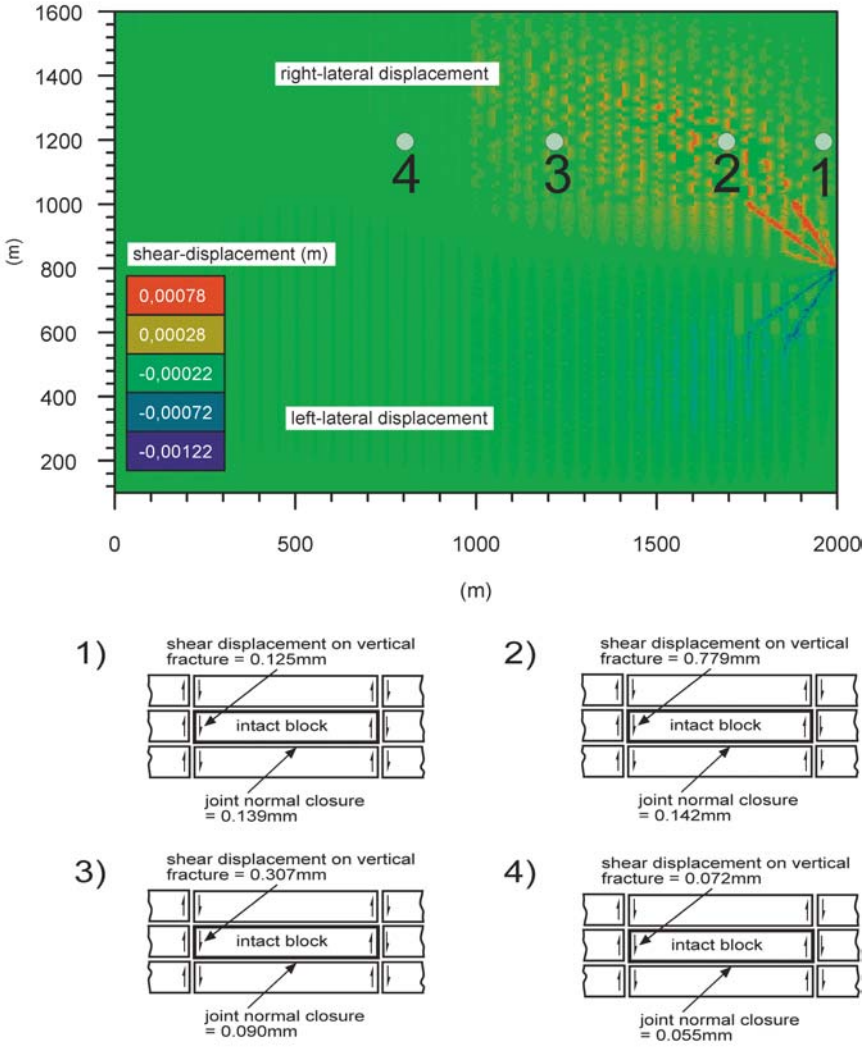

Fig. 14 Shear deformation showing zones of right- or left-lateral displacement for conceptual model 3 (*upper*). Block models showing shear and normal fracture displacements at location numbers 1, 2, 3 and 4 (*lower*)

 DOI 10.1007/s10040-002-0234-4

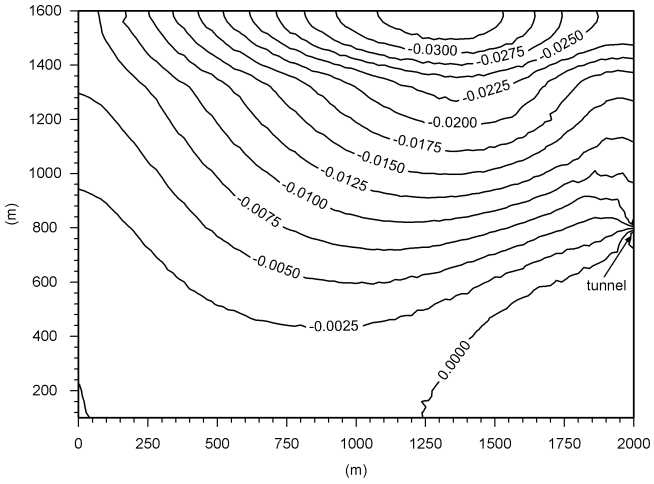

Fig. 15 Vertical subsidence (in metres) for vertical brittle fault zone-controlled model (conceptual model 3)

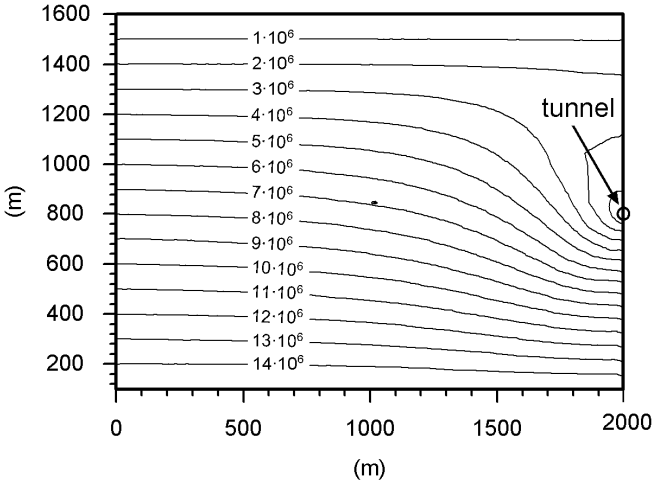

Fig. 16 Pore-pressure distribution (units in Pa) for the fixed water-table condition (boundary condition B)

ues of 1.4 mm. As such, results for deformation model 3 suggest that the point of maximum subsidence may not occur directly above the tunnel (Fig. 15). Vertical fractures, therefore, can affect the shape and location of the settlement trough if vertical displacements are dominated by vertical fracture closure and intact block deformation as opposed to horizontal joint closure (as shown for deformation model 1).

Relatively high inflow rates into the tunnel of 12 l/s/m were modelled at steady state conditions. This is due to the elevated equivalent rock mass hydraulic conductivity, the large tunnel diameter and the 'drainage fractures' implemented in the model. The modelled hydraulic parameters (i.e. inflow rates, water-table drawdown) are typical for conductive brittle fault zones in the Gotthard region.

Boundary Condition 'B': Fixed Water Table

Models in which pore pressures were fixed along the top boundary (i.e. fixed water table) roughly show a 20–50% reduction in subsidence magnitudes. Figure 16 shows the pore-pressure distribution for these models subsequent to tunnel drainage. The extent and shape of the reduced pore-pressure zone is strongly controlled by the hydraulic apertures of the horizontal and vertical fractures, as well as the aperture-ratio between them. Thus, surface deformation depends largely on these hydraulic parameters for the case of a fixed water table. Subsidence results from these models also show a completely different distribution of vertical displacements from that of the 'water table drawdown' series of models (i.e. boundary condition A). Instead of an extensive settlement trough along most of the model's surface, the subsidence profile calculated for the fixed water-table models is generally more restricted to the area directly overlying the tunnel (Fig. 17).

Adopting the same fixed pore-pressure boundary condition, the finite-element solution for the continuum

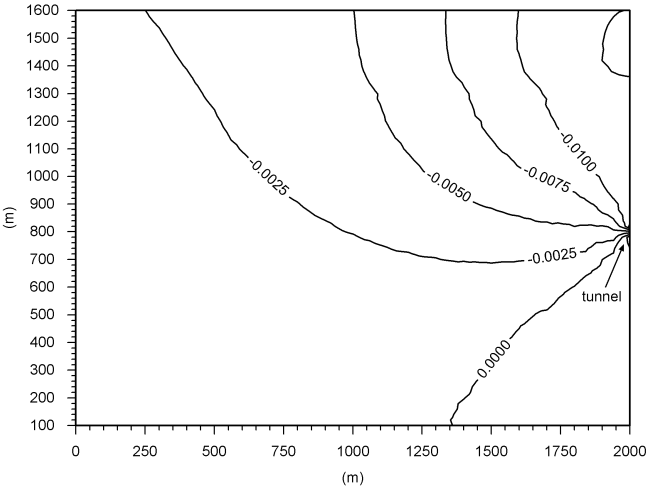

Fig. 17 Vertical subsidence (in metres) for the fixed water-table condition (boundary condition B)

case, deformation model 4, showed a similar drained pore-pressure redistribution pattern (Fig. 18). Likewise, the distribution of vertical displacements showed similar trends with respect to predicting a more narrow subsidence trough largely confined to the region directly above the tunnel. The maximum settlement calculated for the continuum case, for the given material properties and permeability, was 2.5 cm (Fig. 19). An added advantage afforded by means of using the finite-element consolidation solution is the ability to model the time-dependent response. The model was solved assuming a 10-day time step, with results showing that steady-state conditions were reached after approximately 200 days (Fig. 20). Further investigations with respect to the 2-D and 3-D evolution of the surface settlements generated through the poro-elastic response above the Gotthard tunnel are part of an on-going study.

 DOI 10.1007/s10040-002-0234-4

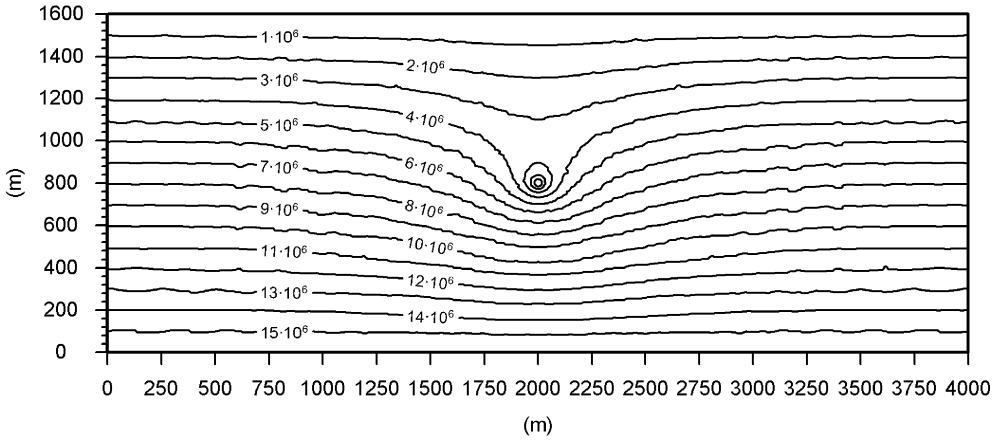

Fig. 18 Pore-pressure distribution (units in Pa) calculated for the continuum intact rock matrix case

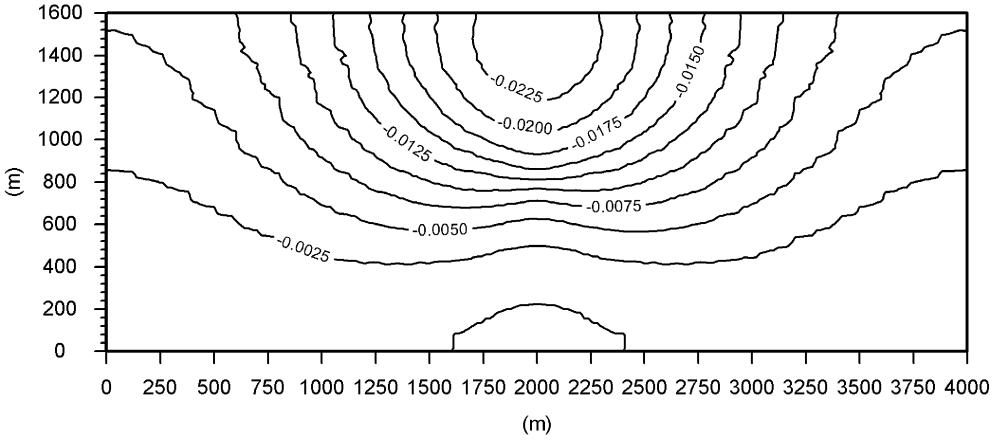

Fig. 19 Vertical subsidence (in metres) calculated for the continuum intact rock matrix case (conceptual model 4)

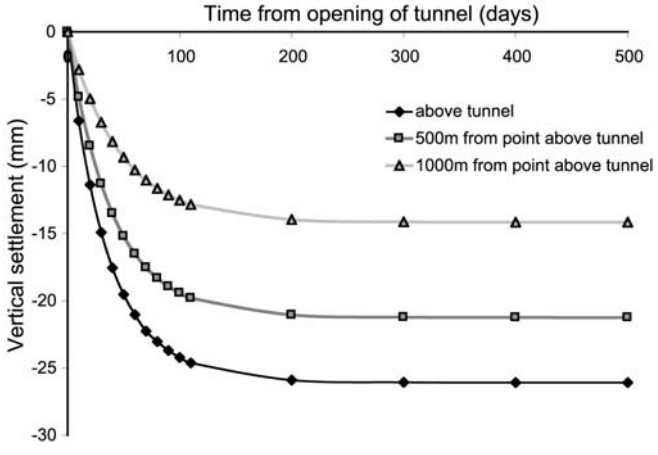

Fig. 20 Transient response of vertical displacements with time for the continuum intact rock matrix case

Summary and Conclusion

Several deformation models have been presented to explain possible mechanisms acting to promote surface settlements in crystalline rock masses through deep tunnel drainage. Models involving elements of fracture drainage and consolidation were studied using distinct-element modelling techniques. Similar models concentrating on the poro-elastic response of the intact rock matrix were solved using finite-element continuum modelling.

Preliminary distinct-element results suggest that the measured settlements of 12 cm in a fractured granitic rock mass above the Gotthard tunnel cannot be explained easily by fracture deformation alone. Only by decreasing the joint spacing or normal stiffness to values below those observed in the field or in the lab is it possible to model such large magnitudes of subsidence. However, continuum models suggest that the contributing influence of consolidation of the intact rock mass must also be considered. Table 4 summarises the modelled magnitudes of vertical displacement for the four different conceptual models presented. These results show that, in terms of the underlying coupled hydromechanical mechanisms, it is the combined influence of vertical and horizontal fractures and the intact rock matrix that can act to generate surface settlements as a consequence of deep tunnel drainage. Further investigations within the framework of this study are now focusing on the influence of inclined joints and fault zones, as well as the sensitivity of the different deformation models to other key input parameters (e.g. horizontal to vertical stress ratio, permeability, etc.). Additionally, numerical modelling will be applied to reproduce the measured settlement trough in its shape and quantity and also the distribution of water

 DOI 10.1007/s10040-002-0234-4

Table 4 Summary of results showing maximum settlements modelled and point of maximum settlement relative to surface point directly above the tunnel

Deformation models	Condition A Maximum settlement (cm)	Condition B Maximum settlement (cm)
1. Horizontal joints dominate	2.5	1.3
2. Vertical joints dominate	3	2.4
3. Vertical faults dominate	3.6[a]	2.4[a]
4. Intact rock matrix dominates	No data	2.5

[a] Maximum settlements not located directly above tunnel, but 650- and 450-m displaced from point directly above the tunnel

inflow rates into the tunnel at the particular site in the Gotthard region.

Acknowledgements The authors would like to thank the maintenance team of the Gotthard A2 highway tunnel for their kind support of this work and the AlpTransit Gotthard AG for the permission to publish the settlement data. Thanks are also extended to Dr Keith Evans, ETH Zürich, and Dr Giovanni Lombardi, Lombardi Consulting, for their input during numerous discussions.

References

Bandis SC, Lumsden AC, Barton NR (1983) Fundamentals of rock joint deformation. Int J Rock Mech Min Sci Geomech Abstr 20(6):249–268

Bart M, Sibai M, Shao JF (2000) Modelling of hydromechanical behaviour of rock joints under normal stress. Proceedings of the ISRM Regional Symposium EURock, Aachen, pp 591–596

Detournay E, Cheng AHD (1993) Fundamentals of poro-elasticity. In JA Hudson (ed) Comprehensive rock engineering: principles, practice and projects, vol 2, pp 113–171

Infanti N, Kanji MA (1978) In situ shear strength, normal and shear stiffness determinations at Agua Vermelha Project. Proceedings of the 3rd International Congress IAEG, pp 175–183

Itasca (1999) UDEC Universal distinct element code, version 3.1. Itasca Consulting Group, Minneapolis

Kohl T, Signorelli S, Rybach L (2000) Constraints on palaeotopography by revised apatite fission track uplift rates. European Geophysics Society 25th General Assembly, vol 2

Loew S (2001) Natural groundwater pathways and models for regional groundwater flow in crystalline rocks. Proceedings of the 31st International Congress IAH, Munich

Loew S (2002) Groundwater hydraulics and environmental impacts of tunnels in crystalline rocks. Proceedings of the 9th International Congress IAEG, Durban

Lombardi G (1988) Les tassements exceptionnels au barrage de Zeuzier. Publ Soc Suisse Mécanique Sols Roches 118:39–47

Lutzenkirchen V (2002) Structural geology and hydrogeology of brittle fault zones in the central and eastern Gotthard Massif, Switzerland. PhD Thesis, ETH Zuerich

Majer EL, Myer, LR, Peterson Jr. JE, Karasaki K, Long JCS, Martel SJ, Blümling P, Vomvoris S (1990) Joint seismic, hydrogeological, and geomechanical investigations of a fracture zone in the Grimsel Rock Laboratory, Switzerland. NAGRA-DOE Cooperative Project Report NDC #14

Makurat A, Barton N, Tunbridge L, Vik G (1990) The measurement of the mechanical and hydraulic properties of rock joints at different scales in the Stripa project. In: Barton, Stephansson (eds) Rock Joints. pp 541–548

Martin CD, Davison CC, Kozak ET (1990) Characterizing normal stiffness and hydraulic conductivity of a major shear zone in granite. In: Barton and Stephansson (eds) Rock Joints. pp 549–556

Nur A, Byerlee JD (1971) An exact effective stress law for elastic deformation of rock with fluids. J Geophys Res 76(26):6414–6419

Pratt HR, Swolfs HS, Brace WF, Black AD, Handin JW (1977) Elastic and transport properties of an in situ jointed granite. Int J Rock Mech Min Sci Geomech Abstr 14:34–45

Pyrak-Nolte LJ, Morris JP (2000) Single fractures under normal stress: The relation between fracture specific stiffness and fluid flow. Int J Rock Mech Min Sci 37:245–262

Robin P-YF (1973) Note on effective pressure. J Geophys Res 78(14):2434–2437

Sun Z, Gerrard C, Stephansson O (1985) Rock joints compliance tests for compression and shear loads. Int J Rock Mech Min Sci Geomech Abstr 22:197–213

VIPS (2001) VISAGE vectorial implementation of structural analysis and geotechnical engineering, version 8.0. Vector International Processing Systems Ltd, Winkfield, Windsor, UK

Zangerl C, Eberhardt E, Loew S, (2001) Analysis of ground settlement above tunnels in fractured crystalline rocks. Proceedings of the ISRM Regional Symposium Eurock, Espoo, pp 717–722

 DOI 10.1007/s10040-002-0234-4